Engineered Science
DOI: https://dx.doi.org/10.30919/es1040

Design of a Patch Antenna for High-Gain Applications Using One-Dimensional Electromagnetic Band Gap Structures

Sara Said,[1, 2,*] Ouafae El melhaoui,[1] Yassmina Guetbach,[2] Elhadi Baghaz[3] and Ahmed Faize[4]

Abstract

This research paper delves into the precise determination of the band gap within one-dimensional Electromagnetic Band Gap (1D-EBG) structures, employing the Transfer matrix method as a key analytical tool. Following this investigation, a groundbreaking design of a 1D-EBG antenna is introduced with the specific goal of augmenting directivity at the frequency of 3.5 GHz, strategically catering to WiMax applications. The primary objective of this study is to validate the proposed methodology and evaluate the performance of the directive 1D-EBG antenna precisely at the resonant frequency of 3.5 GHz, ensuring optimal adaptation. Furthermore, the paper highlights the significant influence of dielectric substrates in achieving a noteworthy up to 20 dB improvement in directivity. The emphasis is placed on showcasing the impact of these substrates in optimizing the antenna's performance. The novel 1D-EBG antenna, as proposed, exhibits an impressive 14 dBi gain enhancement in comparison to a conventional antenna lacking EBG. This remarkable improvement is coupled with an exemplary level of adaptation, affirming the efficacy of the designed antenna for practical applications. The study not only validates the proposed approach but also underscores the potential of 1D-EBG structures in significantly advancing the performance of antennas, particularly in the context of WiMax applications.

Keywords: Electromagnetic band-gap 1D-EBG; Patch antenna; High directivity characteristics.
Received: 06 November 2023; Revised: 22 November 2023; Accepted: 25 November 2023.
Article type: Research article.

1. Introduction

The introduction to a topic as captivating as high-gain antennas and techniques to enhance their directivity provides an intriguing overview of advancements in the field of wireless communications. High-gain antennas have played a pivotal role in enhancing the performance of modern communication systems, enabling more robust and longer-distance connections. In this introduction, we will delve into the concept of high gain in the context of antennas, as well as the innovative methods employed to enhance their directivity. The essence of high gain lies in an antenna's ability to concentrate emitted energy in a specific direction, thereby amplifying apparent power in that direction compared to an isotropic antenna.[1] Applications ranging from space communications to wireless networks and remote sensing demand antennas capable of achieving higher gain levels to overcome physical obstacles and minimize signal disruptions. To achieve high gain, various techniques have been developed and refined over the years. Among them, we find the utilization of parabolic dish antennas,[2,3] horn antennas,[4,5] slot antennas,[6-9] and more. These traditional concepts have evolved as new technologies emerge, including phased array antennas,[10-12] which leverage constructive interference to steer energy in a specific direction. Similarly, fractal antenna structures[13] and electromagnetic bandgap (EBG) materials[14-16] have paved the way for innovative possibilities in enhancing gain and directivity. In this exploration, we will review these various methods and discuss their effectiveness, advantages, and potential challenges. We will also address the practical implications of using high-gain antennas in areas such as 5G networks,[17,18] satellite communications, and high-resolution radars. Ultimately, this introduction provides a glimpse into the advancements in high-gain antennas and the impact they have on how we stay connected and interact with

[1] *Research Center, High Studies of Engineering School, EHEI, Oujda, 60000, Morocco.*
[2] *Department of Physics, Faculty of Sciences, University of Mohamed Premier, Oujda, 60000, Morocco.*
[3] *Laboratory of Electronics, Instrumentation and Energetic, Department of physics, Faculty of Sciences, Chouaïb Doukkali University, El Jadida, 24010, Morocco.*
[4] *Department of Physics, Polydisciplinary Faculty, University of Mohamed Premier, Nador, 62000, Morocco.*
**Email:* said.sara63@gmail.com (S. Said)

the world around us. An innovative and promising approach to enhance antenna gain and directivity involves harnessing electromagnetic bandgap (EBG) structures. EBGs are periodic arrangements of dielectric or conductive materials that exhibit frequency bands where electromagnetic wave propagation is strongly attenuated, creating "gaps" in the frequency spectrum. This unique characteristic can be exploited to manipulate and control antenna radiation properties. By incorporating EBG structures into antenna design, it becomes possible to influence how electromagnetic waves propagate and radiate. EBG structures can be utilized in various ways to increase antenna gain and directivity. One common approach is placing EBG structures in close proximity to the radiating element of the antenna. This configuration alters the spatial distribution of currents and electromagnetic fields, potentially leading to improved radiation in a specific direction. Moreover, by adjusting the geometry of EBG structures, it's possible to mitigate undesired secondary lobes in the radiation pattern, thus enhancing directivity. Another innovative strategy relies on leveraging the reflective properties of EBG structures to create virtual "walls" that guide and steer electromagnetic waves in specific directions. These EBG reflectors act as mirrors for the waves, redirecting them with adjusted phases to reinforce radiation in the desired direction. This paper aims to delve deeper into the electromagnetic characteristics of one-dimensional electromagnetic bandgap (1D EBG) structures and their implications for the design of directive antennas. In Section 2, we introduce the transfer matrix method as a means to theoretically ascertain the band gap of the 1D EBG structure and gain insights into its operational behavior. Moving on to Section 3, we proceed with the creation of a 1D EBG antenna design, where we make a pivotal alteration by substituting the symmetry plane presented by the 1D EBG structure with a metallic plane. On this metallic plane, we position an excitation source in the form of a patch. The conclusive findings of this research will be outlined in Section 4.

2. Investigation and setup of the Electromagnetic Band Gap (EBG) structure

Within a system responsible for both receiving and transmitting, S parameters are the most commonly used. The method of matrix for transfer is the simplest way to determine Electromagnetic Band Gaps (EBGs) by calculating the coefficient of reflection Γ and the coefficient of transmission T. This technique finds extensive application in guiding light through layered materials.[19,20] In a structure comprising N layers arranged through the z-direction where the index of refraction remains constant within each layer, a 2x2 transfer matrix (referred to as matrix Mi or specific matrix 1) establishes the connection between electromagnetic fields on the layer's left and right sides, considering both TE and TM modes. Consequently, the objective at hand involves calculating an appropriate transfer matrix for each individual cell.

Let $\overrightarrow{E_l} = E_0 e^{j(\omega t - \vec{k}.\vec{z})}\overrightarrow{e_x}$ be a uniform sinusoidal plane wave with rectilinear polarization along the (ox) axis, propagating in free space along the (oz) axis and normally incident on the flat surface of a dielectric layer (see Fig. 1).

To ascertain the EBG structure band gap, the S-parameters properties are employed, as described in reference.[21] The computation of these parameters is conducted employing approach of the matrix for transfer. The matrix pertaining to each individual layer is denoted by the subsequent Equation 1:

$$M_i = \begin{bmatrix} cos(\delta_i) & j\frac{sin(\delta_i)}{\gamma_i} \\ j\gamma_i\, sin(\delta_i) & cos(\delta_i) \end{bmatrix} \quad (1)$$

With: $\delta_i = dk_i$ and $\gamma_i = \frac{k_i}{\omega}$

The global transfer matrix corresponding to the entire structure, considered as a set of N layers (see Fig. 1), is obtained by taking the product of individual transfer matrices Mi:

$$M = \begin{bmatrix} m_{11} & m_{12} \\ m_{21} & m_{22} \end{bmatrix} = \prod_{i=1}^{n} M_i \quad (2)$$

In the assembly shown in Fig. 1:

$$\begin{bmatrix} E_0 \\ B_0 \end{bmatrix} = \begin{bmatrix} m_{11} & m_{12} \\ m_{21} & m_{22} \end{bmatrix} \begin{bmatrix} E_n \\ B_n \end{bmatrix} \quad (3)$$

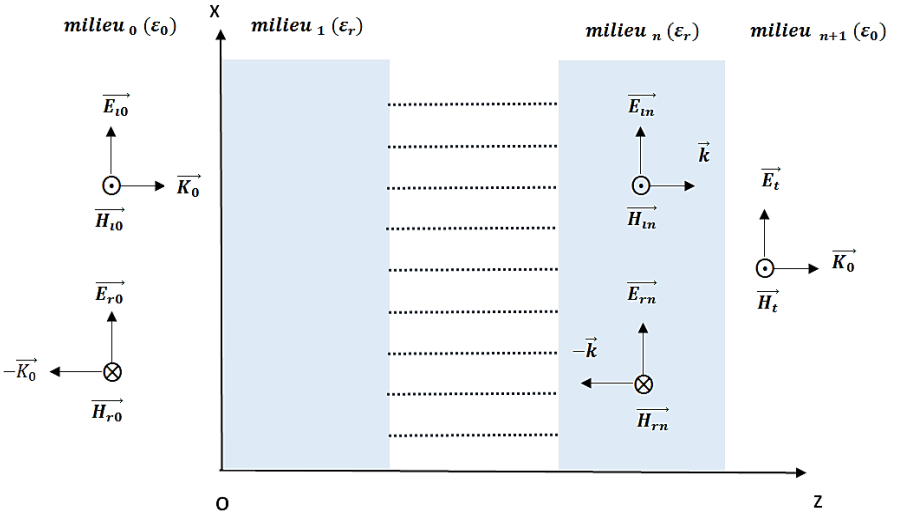

Fig. 1 Stack of N layers.

At the final boundary of the periodic arrangement, the tangential constituents of the electromagnetic field remain consistent.

$$\begin{cases} E_n = E_{n+1} \\ H_n = H_{n+1} = \frac{1}{\eta_{n+1}} E_t \end{cases} \quad (4)$$

Beyond the ultimate interface, the field will solely comprise the elements that have been transmitted (E_t, H_t), given that the structure's excitation originates exclusively from the left side.

$$\begin{cases} E_{n+1} = E_t \\ H_{n+1} = H_t = \frac{1}{\eta_{n+1}} E_t = \frac{1}{\eta_0} E_t \end{cases} \quad (5)$$

The matrix (3) is written as follows:

$$\begin{bmatrix} E_0 \\ B_0 \end{bmatrix} = \begin{bmatrix} m_{11} & m_{12} \\ m_{21} & m_{22} \end{bmatrix} \begin{bmatrix} E_t \\ B_t \end{bmatrix} \quad (6)$$

However, it is known that:

$$\begin{cases} E_0 = E_{i0} + E_{r0} \\ H_0 = \frac{1}{\eta_0}(E_{i0} - E_{r0}) \end{cases} \quad (7)$$

The equations (5 and 7) allow us to write the matrix (6) in the following form:

$$\begin{bmatrix} E_{i0} + E_{r0} \\ \frac{\mu_0}{\eta_0}(E_{i0} + E_{r0}) \end{bmatrix} = \begin{bmatrix} m_{11} & m_{12} \\ m_{21} & m_{22} \end{bmatrix} \begin{bmatrix} E_t \\ \frac{\mu_0}{\eta_0} E_t \end{bmatrix} \quad (8)$$

Finally, we find:

$$\begin{bmatrix} E_{i0} + E_{r0} \\ \Gamma_0(E_{i0} + E_{r0}) \end{bmatrix} = \begin{bmatrix} m_{11} & m_{12} \\ m_{21} & m_{22} \end{bmatrix} \begin{bmatrix} E_t \\ \Gamma_0 E_t \end{bmatrix} \quad (9)$$

With $\Gamma_0 = \frac{n_0}{c}$, where n_0 represents the refractive index of the medium at the boundaries of the unit cell; in this instance, n_0 is set to 1.

After substituting the expressions of E_{i0} and E_{r0}, we observe that $E_i = E_{i0}$ and $E_r = E_{r0}$. Thus, we obtain:

$$\begin{cases} E_t = \frac{2\Gamma_0}{m_{11}+\Gamma_0^2 m_{12}+m_{21}+\Gamma_0 m_{22}} E_i \\ E_r = \frac{\Gamma_0 m_{11}+\Gamma_0^2 m_{12}-m_{21}+\Gamma_0 m_{22}}{\Gamma_0 m_{11}+\Gamma_0^2 m_{12}+m_{21}+\Gamma_0 m_{22}} E_i \end{cases} \quad (10)$$

The periodic arrangement is exposed to a plane wave that propagates perpendicular to its surface at the frequency f_0. The waves undergoing diffraction are described by their respective coefficients denoting transmission (T) and reflection (Γ). The approach for computing these coefficients (T and Γ) is depicted in Fig. 2.

The point of observation situated behind the photonic structure where the transmitted field exists for calculate the coefficient of transmittance (T). In order to derive the coefficient of reflection (Γ), the observation point is situated within the region where the reflected field exists, as depicted Fig. 2:

$$\Gamma = \frac{E_{reflected}}{E_{incident}} \quad (11)$$

$$T = \frac{E_{transmitted}}{E_{incident}} \quad (12)$$

According to (10), the coefficients for reflection and transmission corresponding to the superposition of all layers are expressed as follows:

$$\Gamma = \frac{\Gamma_0 m_{11}+\Gamma_0^2 m_{12}-m_{21}+\Gamma_0 m_{22}}{\Gamma_0 m_{11}+\Gamma_0^2 m_{12}+m_{21}+\Gamma_0 m_{22}} \quad (13)$$

$$T = \frac{2\Gamma_0}{\Gamma_0 m_{11}+\Gamma_0^2 m_{12}+m_{21}+\Gamma_0 m_{22}} \quad (14)$$

To graphically determine the band gap, a Bragg mirror is studied, composed of six dielectric plates with a permittivity $\varepsilon_r = 10.2$ and an thickness $d = \lambda_g/4$ corresponding to the frequency f_0=3.5 GHz. These dielectric plates are interspersed by air layers with a dimension of $d_0 = \lambda_0/4$. As illustrated in Fig. 3, the periodic arrangement has the ability to achieve complete reflection within specific frequency ranges. Within these ranges, the transmission coefficient (as defined by equation 14) approaches near-zero values (much less than -20 dB), while the reflection coefficient (as defined by equation 13) equals 1 (equivalent to 0 dB).

The number of periods of the EBG structure of the dielectric material used determines the depth of the band gap. Fig. 4 depicts the impact of varying the number of periods (plates) within the structure with $\varepsilon_r = 10.2$. It is evident that the depth of the transmission well increases as the number of periods increases. This is due to multiple reflections on the dielectric plates.[7]

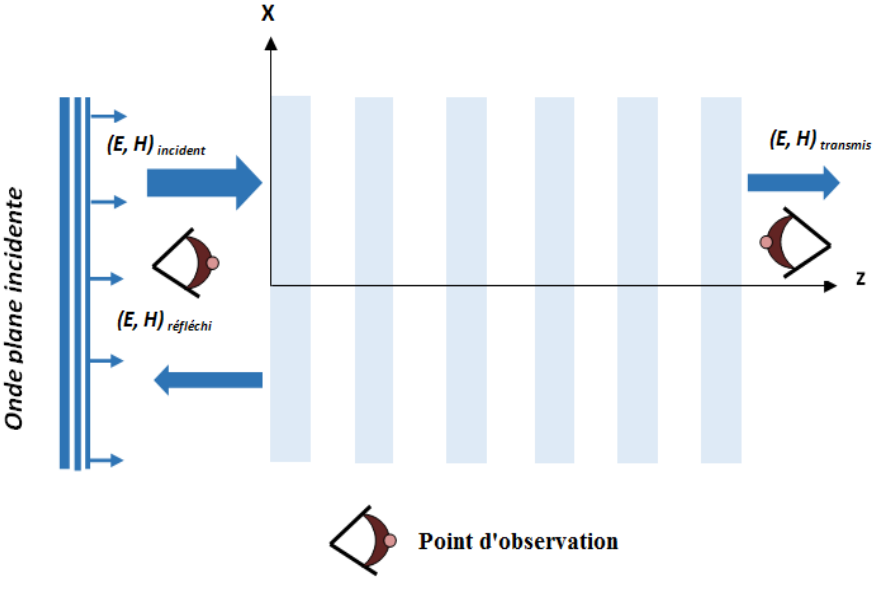

Fig. 2 Locations of measurement points used to compute the transmission and reflection coefficients.

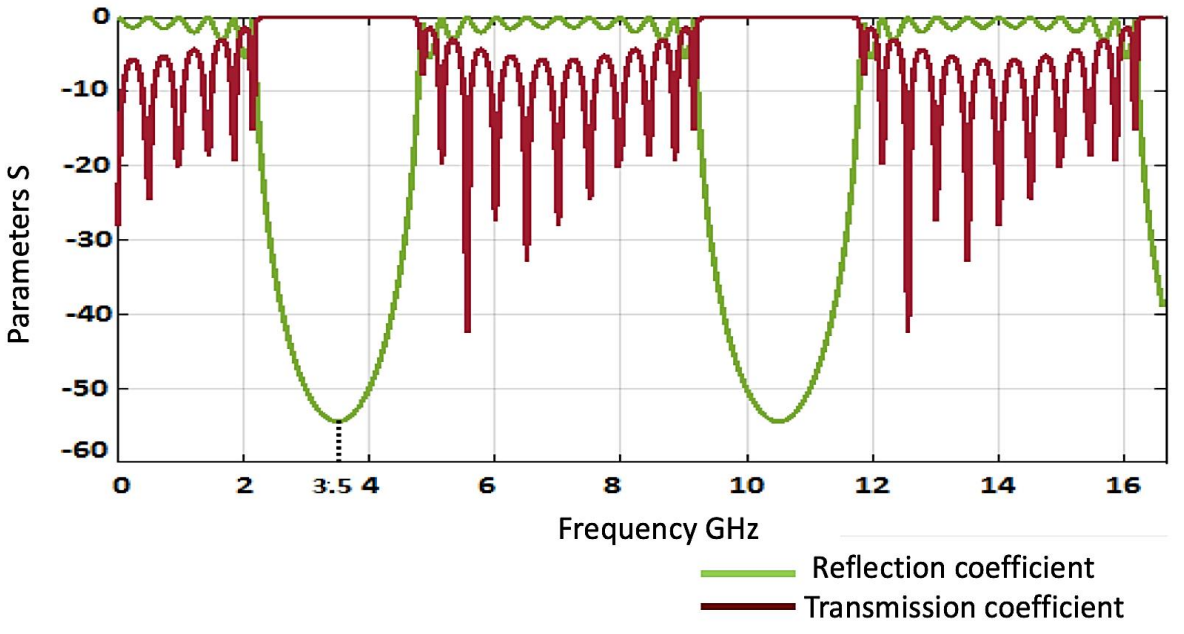

Fig. 3 S-parameters under normal incidence.

The proposed Electromagnetic Band Gap (EBG) configuration is constructed using alternating layers of Neltec material with a relative permittivity (ε_r) of 2.6, along with layers of air. This arrangement is visually depicted in Fig. 5a. When a λ_0 disturbance, aligned with the operational frequency of 3.5 GHz, is introduced at the center of the EBG structure, see Fig. 5a, a thin band of transmission forms in the center of the band gap region. This phenomenon is illustrated in Fig. 5b, it becomes evident that the transmission peak symmetrically resides within the band gap. This symmetry arises because the frequency of the peak is inherently connected to the discrepancy in periodicity between the layers.

3. The EBG antenna configuration

The symmetry plane depicted in Fig. 5a can be substituted with a ground plane (or metal plane). This alteration is supported by the electrical field mapping, which indicates the annulment of the tangential element of the electric field along this symmetrical illustration.[22] As a consequence, upon applying the electric image theory, the characteristics of the structure bisected into two halves relative to the ground plane closely resembles that of the defected EBG structure. In this context, an excitation source is located at the ground plane, leading to the creation of an antenna referred to as the EBG antenna. The antenna comprises a ground plane with an excitation patch situated along the symmetry plane of the EBG structure. The placement of the excitation patch is at the center of the fault as defined by Thevenot *et al*.[23]

In Fig. 6a, the depiction showcases the EBG (1-D) antenna configuration. This setup is comprised of three dielectric

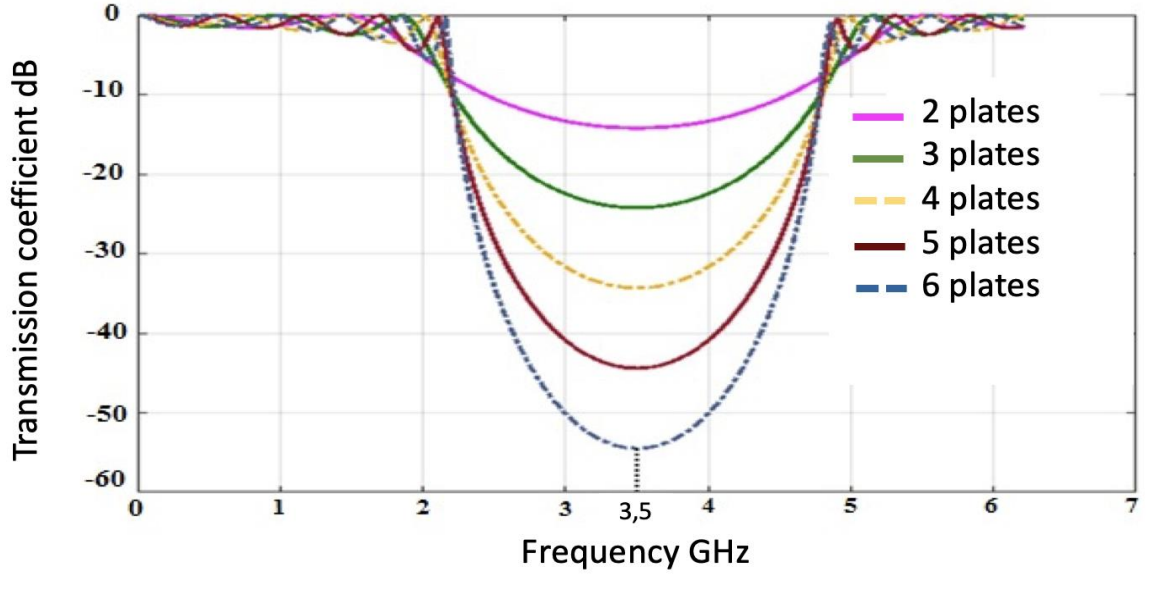

Fig. 4 The quantity of periods effect on the coefficient of transmittance of a EBG structure with $\varepsilon_r = 10.2$.

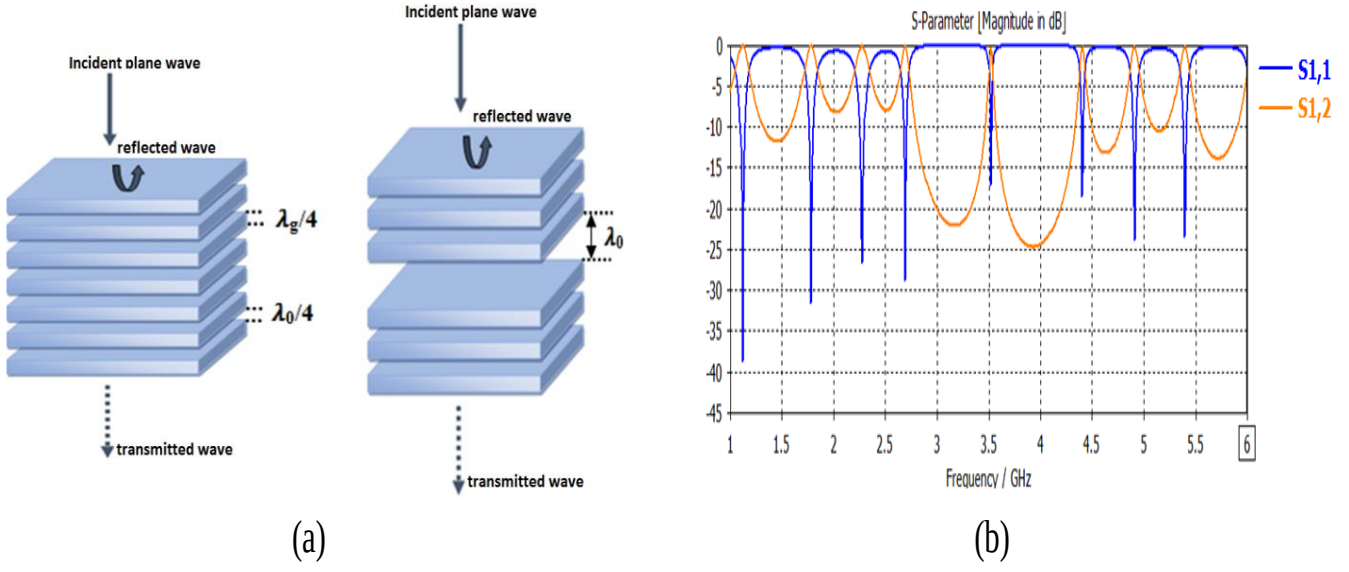

Fig. 5 (a) Periodic 1-D EBG structure (b)Transmission coefficient (orange curve) and reflection (blue curve) of the EBG structure with default.

layers of Neltec NY9260, each measuring 13.30 mm in thickness. These layers are positioned at a distance of 41.85 mm from the ground plane and are accompanied by an excitation source. Moving on to Fig. 6b, it provides insight into the return loss characteristics of the EBG 1-D antenna. This data demonstrates that both the antenna configurations, with and without the EBG structure, are effectively suited and encompass the intended WiMax frequency band.

Upon examining Fig. 7 and Fig. 8 the subsequent observations, it becomes evident that the introduction of the EBG structure contributes to a marked enhancement in antenna performance. Notably, the radiation pattern exhibits a substantial augmentation in its directional characteristics, indicative of a significant overall improvement.

Table 1 allows us to conclude that by using 1D-EBG structures, a significant improvement in directivity of 14 dBi is achieved compared to an antenna without EBG, and very good matching is obtained.

Table 2 outlines a comprehensive comparison between our study and several antennas discussed in the existing literature. The summarized data unmistakably underscores the superiority of our employed technique in enhancing directivity.

Table 1. Comparison between the antenna with and without 1D-EBG structure.

Antenna	Without EBG	With EBG
Frequency (GHz)	3,5	3,49
Reflection Coefficient (dB)	-24	-33
Directivity (dBi)	6	20

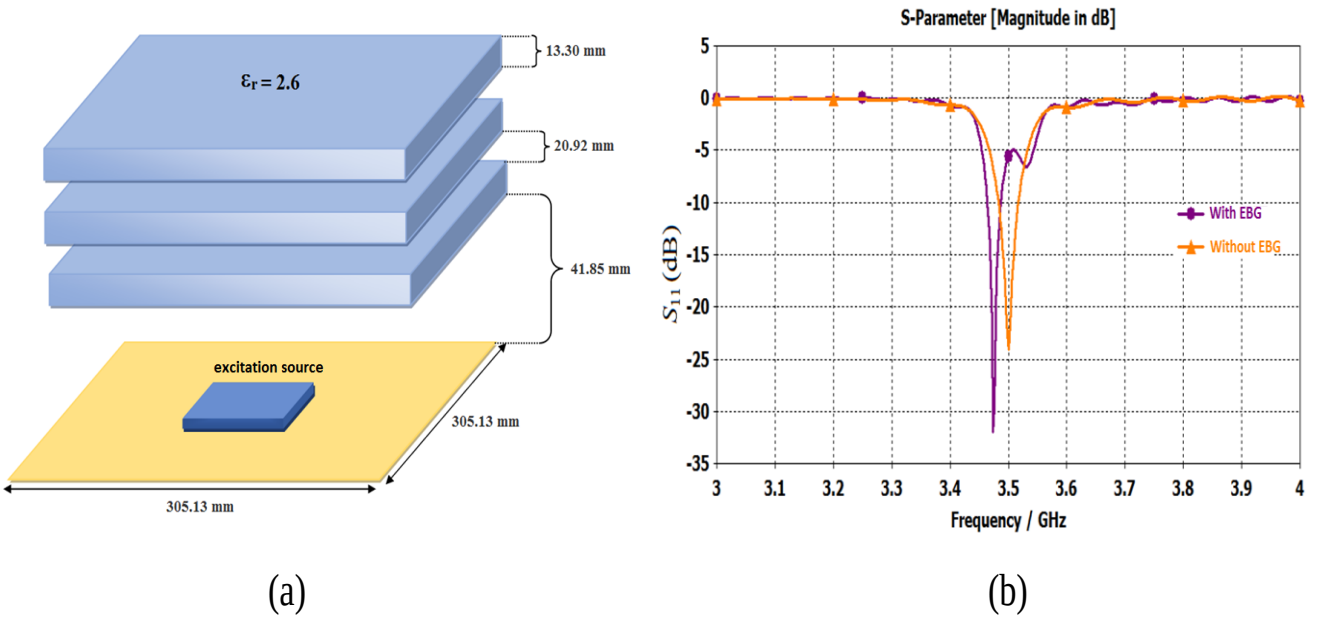

Fig. 6 (a) EBG antenna design, (b) The antenna's reflection coefficient S11 is measured both with and without EBG.

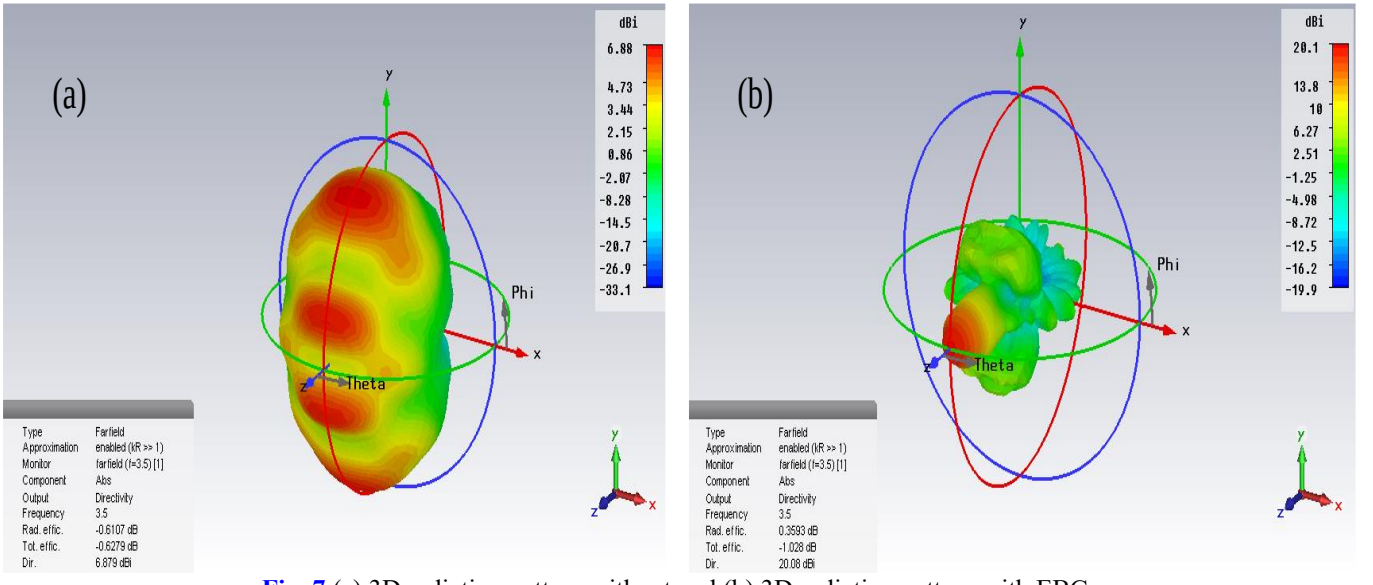

Fig. 7 (a) 3D radiation pattern without and (b) 3D radiation pattern with EBG.

Table 2. Antenna under consideration in contrast to the currently employed reference antenna.

References	Resonance frequency GHz	Directivity (dBi)	Reflection coefficient (dB)	Employed Techniques
This Work	3.5	20	-33	1D-EBG
2021[24]	3.5	7.85	-25	Metasurface as Superstrate
2023[25]	9. 86	8,36	-26,17	Metamaterial superstrate
2022[26]	5,8	14,6	-32	Lens antenna
2022[27]	3,5	7,38	-26	TModd-0 modes
2022[28]	2.74	9.28	--	Antenna with MM Reflector
2023[29]	9.97	8,36	-26,17	metamaterial superstrate
2023[30]	2,6	6,1	-10	Circularly Polarized Antenna

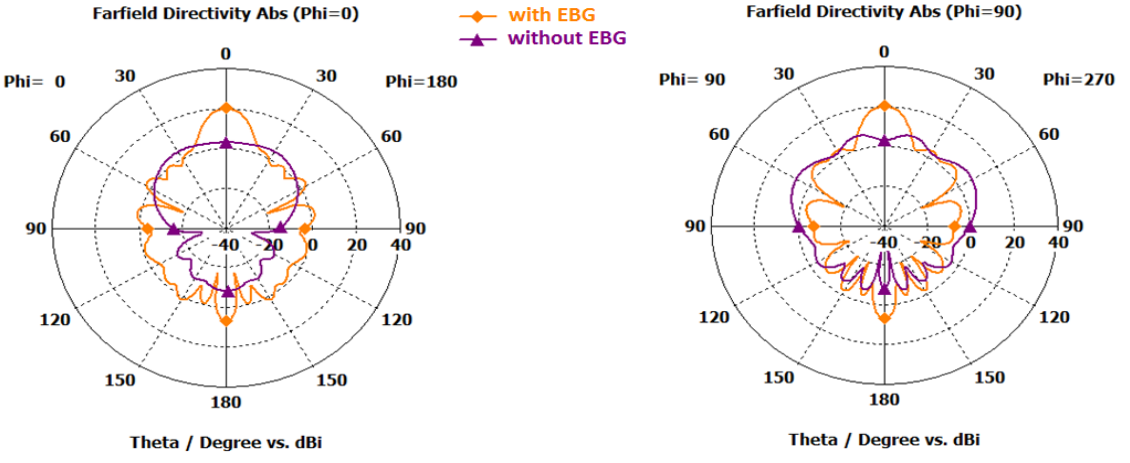

(a) (b)

Fig. 8 The radiation pattern of the dipole antenna with and without EBG is analyzed at 3.5 GHz in both the horizontal and vertical sections, considering two specific angles: (a) phi=0 and (b) phi=90.

4. Conclusion

In this study, our focus centered on the creation of a planar 1D EBG antenna optimized for the 3.5 GHz frequency, tailored to the WiMax bands. Initially, we formulated a method to theoretically ascertain the band gap and gain insight into its operational mechanics. Subsequently, we embarked on the design of a 1D EBG antenna, a process involving the replacement of the initially presented symmetry plane with a metallic plane. On this plane, an excitation source, in the form of a patch, was meticulously positioned. The integration of 1D EBG structures atop the patch antenna yielded a compelling outcome an impressive surge in directivity, approximating a remarkable 20 dB enhancement compared to the EBG-less counterpart, which exhibited a directivity of 6 dB.

Conflict of Interest

There is no conflict of interest.

Supporting Information

Not applicable.

References

[1] Y. B. Nechaev, I. W. peshkov, Evaluation of the influence of directivity factor of directive elements of conformal antenna arrays on the performances of Azimuth-elevation DOA estimation, 2017 Progress In Electromagnetics Research Symposium-Spring(PIERS), IEEE, 2017, 490-495, doi: 10.1109/PIERS.2017.8261791.

[2] B. P. A. Mahatmanto, C. Apriono, Gain performance analysis of a parabolic reflector fed with a rectangular microstrip array antenna, 2020 IEEE International Confererence on Industry 4.0, Artificial Intelligence and Communications Technology (IAICT). IEEE, 2020, 142-145, doi: 10.1109/IAICT50021.2020.9172035.

[3] C. J. Lee, P. C. Tseng, W. C. Wang, Y. H. Liou, Y. T. Cheng, C. N. Kuo, Design and fabrication of a sub-thz co-reflectively curved patch-reflector antenna array for gain enhancement and near field focusing, In 2023 IEEE 73rd Electronic Components and Technology Conference (ECTC), IEEE, 2023, 504-509.

[4] H. Eskandari, J. L. Albadalejo-Lijarcio, O. Zetterstrom, T. Tyc, O. Quevedo-Teruel, H-plane horn antenna with enhanced directivity using conformal transformation optics, *Scientific Reports*, 2021, **11**, 14322, doi: 10.1038/s41598-021-93812-6.

[5] H. Eskandari, T. Tyc, J.L, Albadalejo-Lijarcio, O. Zetterstrom, O. Quevedo-Teruel, Design of an impedance-matched horn antenna with enhanced directivity using conformal transformation optics, 2020 14th European Conference on Antennas and Propagation (EuCAP), Copenhagen, Denmark, 2020, 1-4, doi: 10.23919/EuCAP48036.2020.9135870.

[6] J. F. Lin, Q. X. Chu, Enhancing gain of ring slot antennas with shorting strips, *IEEE Transactions on Antennas and Propagation*, 2019, **67**, 4397-4405, doi: 10.1109/TAP.2019.2908107.

[7] R. Bayderkhani, K. Forooraghi, E. Arnieri, B. Abbasi-Arand and B. S. Virdee, Analysis of an integrated lens antenna fed by SIW slot array using a hybrid MoM–PO method, *International Journal of Microwave and Wireless Technologies*, 2017, **9**, 463-468, doi: 10.1017/S1759078715001713.

[8] T. Jaschke, B. Rohrdantz, H. K. Mitto, A. F. Jacob, Ultrawideband SIW-Fed Lens Antenna, *IEEE Antennas and Wireless Propagation Letters*, 2017, **16**, 2010-2013, doi: 10.1109/LAWP.2017.2693179.

[9] V. M. Pepino, A. F. da Mota, A. Martins, B.-H. V. Borges, 3-D-printed dielectric metasurfaces for antenna gain improvement in the ka-band, *IEEE Antennas and Wireless Propagation Letters*, 2018, **17**, 2133-2136, 10.1109/LAWP.2018.2860521.

[10] S. Said, M. Grari, Y. Guetbach, A. Es-Salhi, Z.C. Allah, B. Elhadi, A. Faize, A new hybrid method for mutual coupling minimization of an antenna array, *International Journal of Electrical and Computer Engineering*, 2023, **13**, 2299-2308, doi: 10.11591/ijece.v13i2.pp2299-2308.

[11] S. Said, A. Es-Salhi, M. Elhitmy, Reduction of mutual coupling between radiating elements of an array antenna using EBG electromagnetic band structures, *International Journal of Electrical and Electronic Engineering & Telecommunications*, 2021, **10**, 91-98, doi: 10.18178/ijeetc.10.2.91-98.

[12] M. K. Pote, P. Mukherji, A. Sonawane, Design of 5G Microstrip patch array antenna for gain enhancement, *Journal of Integrated Science and Technology,* 2022, **10**, 198-203.

[13] N. RAO, Gain Enhancement of Miniaturized Fractal Antenna with Help of Complementary Fractal Lens, *Wireless Personal Communications*, 2022, **123**, 229-240, doi: 10.1007/s11277-021-09128-1.

[14] A. Smida, Gain enhancement of dielectric resonator antenna using electromagnetic bandgap structure, Computers, Materials & Continua, 2022, **71**, 1613-1623, doi: 10.32604/cmc.2022.022289.

[15] S. Dey, K. Ashok, H. Sreemoolanadhan, F. B. Babu, S. Dey, Novel Uniplanar Electromagnetic Bandgap Structure for High Gain Antenna and Filter Designs, 2022 IEEE 19th India Council International Conference (INDICON), Kochi, India, 2022, 1-5, doi: 10.1109/INDICON56171.2022.10040201.

[16] S, Said, A. Es-Salhi, Novel Dual-Band Dipole Antenna Integrated with EBG Electromagnetic Bandgap Structures Dedicated to Mobile Communications, 2019 International Conference on Wireless Technologies, Embedded and Intelligent Systems (WITS), Fez, Morocco, 2019, 1-5, doi: 10.1109/WITS.2019.8723660.

[17] M. Nahas, A super high gain l-slotted microstrip patch antenna for 5G mobile systems operating at 26 and 28 GHz, *Engineering, Technology and Applied Science Research*, 2022, **12**, 8053-8057, doi: 10.48084/etasr.4657.

[18] A. Kapoor, P. Kumar, R. Mishra, High gain modified Vivaldi vehicular antenna for IoV communications in 5G

network, *Heliyon*, 2022, **8**, E09336, doi: 10.1016/j.heliyon.2022.e09336.
[19] J. N. Winn, Y. Fink, S. Fan, J. D. Joannopoulos, Omnidirectional reflection from a one-dimensional photonic crystal, *Optics Letters*, 1998, **23**, 1573-1575, doi: 10.1364/OL.23.001573.
[20] S. Mishra, S. Satpathy, One-dimensional photonic crystal: the Kronig-Penney model, *Physical Review B*, 2003, **68**, 045121, doi: 10.1103/physrevb.68.045121.
[21] A. Kaabal, B. El Jaafari, S. Ahyoud, & A. Asselman, Design of EBG antenna with multi-sources excitation for high directivity applications, *Procedia Manufacturing*, 2018, **22**, 598-604, doi: 10.1016/j.promfg.2018.03.087.
[22] R. M. Hashmi, B. A. Zeb, K. P. Esselle, Wideband high-gain EBG resonator antennas with small footprints and all-dielectric superstructures, *IEEE Transactions on Antennas and Propagation*, 2014, **62**, 2970-2977, doi: 10.1109/tap.2014.2314534.
[23] M. Thevenot, C. Cheype, A. Reineix, B. Jecko, Directive photonic-bandgap antennas, *IEEE Transactions on Microwave Theory and Techniques*, 1999, **47**, 2115-2122, doi: 10.1109/22.798007.
[24] T. Z. Fadhil, N. A. Murad, M. K. A. Rahim, M.R. Hamid, L.O. Nur, A beam-split metasurface antenna for 5g applications, *IEEE Access*, 2021, **10**, 1162-1174, doi: 10.1109/ACCESS.2021.3137324.
[25] S. Barman, A. K. Choudhary, T. Moyra, A. Bhattacharjee, A. Debnath, Gain and directivity enhancement of microstrip patch antenna using metamaterial superstrate containing rectangular split ring resonators, 2023, doi: 10.21203/rs.3.rs-1421742/v1.
[26] W. Kim, J. Kim, J. Won, D. Yu, I. J. Yoon, Rapid prototyping of reduced-height dielectric lens with one-take 3d printing for antenna directivity enhancement, *Applied Science*, 2022, **12**, 11811, doi: 10.3390/app122211811.
[27] M. M. Hasan, M. T. Islam, M. Moniruzzaman, M.S. Soliman, A. S. Alshammari, I. I. A. Sulayman, M. S. Islam, Symmetric engineered high polarization-insensitive double negative metamaterial reflector for gain and directivity enhancement of sub-6 ghz 5g antenna, *Materials*, 2022, **15**, 5676, doi: 10.3390/ma15165676.
[28] S. M. Rathod, R. N. Awale, K. P. Ray, S. S. Kakatkar, Directivity enhancement of a circular microstrip antenna with shorting post, *IETE Journal of Research*, 2022, **68**, 504-513, doi: 10.1080/03772063.2019.1612285.
[29] S. Barman, A. Kumar Choudhary, T. Moyra, A. Bhattacharjee, A. Debnath, Gain and Directivity enhancement of microstrip patch antenna using metamaterial superstrate containing rectangular split ring resonators, 2023, doi: 10.21203/rs.3.rs-1421742/v1.
[30] W.-J. Lu, K. Wang, S.-S. Gu, L. Zhu, H.-B. Zhu, Directivity enhancement of planar endfire circularly polarized antenna using V-shaped 1.5-wavelength dipoles, *IEEE Antennas and Wireless Propagation Letters*, 2019, **18**, 1420-1423, doi: 10.1109/LAWP.2019.2918505.